EUROPEAN ORGANIZATION FOR NUCLEAR RESEARCH

CERN-EP/88-142
14 October 1988

EXPERIMENTAL STUDY OF THE INCLUSIVE η-SPECTRUM FROM $p\bar{p}$ ANNIHILATIONS AT REST IN LIQUID HYDROGEN

L. Adiels[8], G. Backenstoss[2], I. Bergström[8], S. Carius[6,8], S. Charalambous[9], M.D. Cooper[2,6], Ch. Findeisen[2,10], D. Hatzifotiadou[3,9], M. Hugi[2,7], A. Kerek[8], H.O. Meyer[2,5], P. Pavlopoulos[3], J. Repond[1,2], L. Tauscher[2], D. Troester[2], M.C.S.Williams[2,4] and K. Zioutas[9]

ABSTRACT

The inclusive η-momentum spectrum from $p\bar{p}$ annihilations at rest in liquid hydrogen was measured at LEAR. Branching ratios were obtained for $p\bar{p} \rightarrow \eta\omega$ $(1.04^{+0.09}_{-0.10})\%$, $\eta\varrho^0$ $(0.53^{+0.20}_{-0.08})\%$, πa_2 $(8.49^{+1.05}_{-1.10})\%$, $\eta\pi^0$ $(1.33 \pm 0.27) \times 10^{-4}$, and $\eta\eta$ $(8.1 \pm 3.1) \times 10^{-5}$. An upper limit for $p\bar{p} \rightarrow \eta\eta'$ of 1.8×10^{-4} at 95% CL was found. The ratio of the branching ratios is $BR(\eta\varrho)/BR(\eta\omega) = 0.51^{+0.20}_{-0.06}$. For the ratio of branching ratios into two pseudoscalar mesons, we have $BR(\eta\pi^0)/BR(\pi^0\pi^0) = 0.65 \pm 0.14$, $BR(\eta\eta)/BR(\pi^0\pi^0) = 0.39 \pm 0.15$, $BR(\eta\eta')/BR(\pi^0\pi^0) < 0.87$ at 95% CL, and $BR(\eta\eta)/BR(\eta\pi^0) = 0.61 \pm 0.25$.

(Submitted to Zeitschrift für Physik)

1) Now at Argonne National Laboratory, Argonne, Ill., USA.
2) Institute for Physics, University of Basle, Switzerland.
3) CERN, Geneva, Switzerland.
4) Now at the Dept. of Physics, University of California, Davis, Calif., USA.
5) Indiana University, Bloomington, Ind., USA.
6) Los Alamos National Laboratory, Los Alamos, N. Mex., USA.
7) Now at Motor Columbus, Baden, Switzerland.
8) Research Institute of Physics, Stockholm, Sweden.
9) Nuclear and Atomic Physics Dept., University of Thessaloniki, Greece.
10) Now at the Dept. of Physics, University of Wisconsin, Madison, Wis., USA.

1. INTRODUCTION

Experimental information on $p\bar{p}$ annihilation at rest in liquid hydrogen, into channels which contain η's, is rather scarce, especially if more than one neutral particle decaying into γ's is in the final state. The main reason for this is the difficulty to detect γ's in bubble-chamber-like experiments. This paper is devoted to the study of the annihilation channels $p\bar{p} \rightarrow \eta\omega$, $\eta\varrho$, $\eta\pi^0$, $\eta\eta$, and $\eta\eta'$. Of these channels, only $\eta\varrho^0$ has been previously measured [1, 2] . We have also investigated the channel $p\bar{p} \rightarrow \pi a_2(1320)$ through the a_2 decay into $\eta\pi$. Data on this channel are available from earlier experiments [3, 4].

This experiment was carried out at the low-energy antiproton ring (LEAR) at CERN. The η's were measured through their decay into two γ's, which were detected by a large lead-glass array.

2. EXPERIMENTAL SET-UP

The experimental set-up is sketched in fig. 1, and the different components are described below.

2.1 Beam

The experiment used the C1 beam of LEAR at a momentum of 330 MeV/c. The momentum spread was of the order of 0.1%, and the beam diameter in the focus was approximately 8 mm (FWHM). A Plexiglas moderator of 2 mm and a scintillation counter of 1 mm thickness and 20 mm diameter, both placed immediately in front of the liquid-hydrogen target, were traversed by the $\bar{p}$'s before they came to rest in the centre of the target. Incoming $\bar{p}$'s were selected and distinguished from reaction π's by their pulse height in this counter. The low and very well defined momentum of the $\bar{p}$ beam resulted in a longitudinal stop distribution that was determined by range straggling only. Its width was measured to be 1.3 mm (FWHM) of scintillator material, corresponding to 12 mm of liquid hydrogen. The lateral stop distribution was estimated by a Monte Carlo simulation of the slowing-down of $\bar{p}$'s, and was found to be of the order of 8.5 mm (FWHM) in diameter [5] including the lateral beam size. An average stop rate of 40,000 $\bar{p}$'s per second was achieved.

2.2 Target

The liquid hydrogen was contained in a cylindrical Mylar tube of 200 mm length, 50 mm diameter, and 125 μm wall thickness, wrapped in a few layers of superinsulation. The vacuum container consisted of a cylinder of Delite, with a 2 mm wall thickness and an inner diameter of 106 mm. The entrance window for the beam consisted of 125 μm thick Mylar foil. These target dimensions ensured that the $\bar{p}$'s stopped in the hydrogen.

2.3 Charged-particle hodoscope (CPH)

To measure the number of charged particles in an event, the target was surrounded by an array of 20 plastic scintillator strips, each 300 mm long, 20 mm wide, and 5 mm thick, arranged to form a cylinder of inner radius of 60 mm. The scintillator strips had a trapezoidal shape and were separated optically by aluminized Mylar so that the inactive space was reduced to a minimum. Viewed from the centre, the solid angle covered by the CPH is 92.8%. The efficiency of the response of the CPH to a charged particle is estimated to be better than 99%.

2.4 Lead-glass (LG) detector

The γ's from η or π^0 decay were detected by an array of 160 lead-glass blocks, arranged in four adjacent rows of 40 blocks each as indicated in fig. 1. The distance from the target centre to the entrance face of the detector was 800 mm. Each block had an entrance surface of 42×64 mm^2, a rear surface of 64×64 mm^2, and a length of 503 mm. This array spanned an angle of 120° around the target. Details of the set-up are given elsewhere [5–7]. The absolute energy calibration was

obtained from the peak positions in the distribution for the invariant mass of two measured γ's, corresponding to $m_{\gamma\gamma} = m_{\pi^0}$. The γ-energy resolution was obtained from the width of this peak and is $7\%/\sqrt{E_\gamma(\mathrm{GeV})}$ (FWHM) [6].

Two layers of overlapping plastic scintillators, 40 mm wide, 260 mm long, and 5 mm thick, were installed in front of the LG array as shown in fig. 1 in order to distinguish charged particles from γ's.

Details of the readout, the monitoring, and the calibration are given in ref. [6].

2.5 Trigger

For fast-triggering purposes, the analog signal from an LG block was split, one branch going to an ADC, the other branch being used for the trigger. The analog signals of the 40 blocks of each LG row were added, and one LG trigger signal was obtained when the sum of the two inner rows corresponded to an energy of more than 40 MeV and the sum of all four rows to more than 80 MeV. Furthermore, the veto counters of the LG (VL) as well as the 'OR' of the four-column blocks of the LG, corresponding to the same angle ϕ, were processed in a fast logic unit to give a trigger whenever two distinct γ candidates (i.e. separated by at least one empty row) were present. This trigger was obtained after 40 ns. The master trigger consisted of the logical 'AND' of these two LG triggers and the beam counter.

The dead-time due to micro duty-cycle problems (i.e. high instantaneous rates) was 5 to 10%. In total, 5.74×10^9 $\bar{p}$'s could finally be used for the analysis.

3. DATA ANALYSIS

The data collected with the system described above were analysed using the following criteria for recognizing a γ:

i) None of the veto counters in front of the blocks containing a γ shower had fired.

ii) A shower was not spread over more than 15° (i.e. five contiguous LG columns, see fig. 1).

iii) Neighbouring shower maxima were separated by more than 9° (this excludes large shower overlaps but does not affect γ pairs of fast π^0's, the minimum angle between such pairs being always larger than 16°).

iv) The total energy of a shower was at least 10 MeV.

If a shower was accepted, the γ impact point on the LG detector was reconstructed using the topology of the modules having deposited energy and weighted according to this energy. The reconstruction makes use of an energy-dependent algorithm. The angle ϕ and the z-position are reconstructed with the following estimated errors [5, 6]:

$$\sigma_\phi = 0.0152\ (\mathrm{rad}) \quad \text{for} \quad E_\gamma < 210\ \mathrm{MeV} \quad \text{(essentially defined by one LG block),} \tag{1a}$$

$$\sigma_\phi = 0.0070\ (\mathrm{rad})/\sqrt{E_\gamma(\mathrm{GeV})} \quad \text{for} \quad E_\gamma \geq 210\ \mathrm{MeV}\ , \tag{1b}$$

and

$$\sigma_z = 1.73\ (\mathrm{cm}) \quad \text{for} \quad E_\gamma < 170\ \mathrm{MeV} \quad \text{(essentially defined by one LG block)}\ , \tag{2a}$$

$$\sigma_z = 0.71\ (\mathrm{cm})/\sqrt{E_\gamma(\mathrm{GeV})} \quad \text{for} \quad E_\gamma \geq 170\ \mathrm{MeV}\ . \tag{2b}$$

These results were derived from the sharp peak in the angular distribution of the γ's from η decays in the reaction $p\bar{p} \rightarrow \eta\omega$ or $\eta\varrho$ [6].

In order to eliminate γ's that are too close to the boundaries of the LG detector in the z-direction, two z-cuts were applied:

i) The only γ's accepted were those where the major part of the shower energy was deposited in the modules of the inner two rows of the LG detector. This confines the effective detector width to $|z| \leq 6.4$ cm. This condition is henceforth called 'central'.

ii) The only γ's accepted were those where $|z| \leq 9$ cm. This cut condition is called 'total'. It increases the solid angle with respect to (i) but introduces a slight momentum-dependent efficiency, described by

$$\epsilon_z(p) = 0.98 - 0.000175p + 7.5 \times 10^{-8} p^2 \qquad (p \text{ in MeV/c}) . \tag{3}$$

This energy-dependent correction was determined by comparing reconstructed z-positions for γ's with $|z| \leq 6.4$ cm (hence well contained in the detector) with those for peripheral γ's with $|z| > 6.4$ cm.

All γ's of an event were then correlated pairwise to construct their invariant mass $m_{\gamma\gamma}$. In fig. 2 the invariant mass distribution is shown in the region of the η mass. The shape of the η-mass peak is Gaussian with a σ of 23.8 MeV/c^2. Only events with $m_{\gamma\gamma} \geq 400$ MeV/c^2 were accepted. This cut ensured that no η events were thrown away. The remaining events were then subject to a kinematical fit, where the energies of the γ's and their positions were optimized so as to obtain $m_{\gamma\gamma} = m_\eta$. Only events with an arbitrary limit of $\chi^2 \leq 4.45$ were accepted. The result of the fitting was the four-momentum of the η.

In fig. 3 the η momentum spectrum is shown for all accepted η's. The pronounced peak is due to the reactions $p\bar{p} \rightarrow \eta\omega$ and $\eta\varrho$, whilst the shoulder at ≈ 800 MeV/c is due to $p\bar{p} \rightarrow \pi a_2$, with $a_2 \rightarrow \pi\eta$. The lower momentum cut-off is due to the angular acceptance limitations of the LG detector.

The CPH information was used in either of two ways: i) to select final states without charged particles (given the solid angle of the CPH, the probability for two charged particles to escape is less than 1%), or ii) to determine the angle ϕ between the direction of the charged particle and the η in the x-y plane (see fig. 1). The calibration of the positioning of the CPH with respect to the LG detector was obtained from charged particles detected in the CPH and in the LG, and is better than 1°.

4. MONTE CARLO SIMULATION

Monte Carlo simulations of the detector–target configuration were carried out for the purpose of obtaining the absolute acceptance of the system, as well as for determining the correct shapes of the η momentum distributions for the annihilation channels $p\bar{p} \rightarrow \eta\varrho$, $\eta\omega$, and πa_2, which serve as input to the later analysis of the η momentum spectra.

The separation of $\eta\varrho$ from $\eta\omega$ based on a shape analysis alone ($\eta\omega$ leads to a narrow peak in the η momentum spectrum, whilst $\eta\varrho$ leads to a wide peak) cannot be envisaged for two reasons: i) both distributions peak at about the same momentum, and ii) the narrowness of the $\eta\omega$ peak is largely lost because of the limited detector resolution. For these reasons the CPH information had to be used in the evaluation and therefore simulated accordingly, as explained later.

No attempt was made to simulate the continuous background of the η momentum spectrum, since this requires knowledge of all annihilation channels, including all intermediate resonances.

The simulations were done using only the geometrical data of the detector, as well as the energy and spatial resolutions discussed above [see eqs. (1) and (2)]. No attempt was made to simulate the electromagnetic shower. The conditions applied were the same as those for the data (see section 3). Kinematical fits were done in order to check the errors for the different measured quantities, as discussed above. The momentum resolution obtained for the $\eta\omega$ peak is $\sigma_p/p = 2.4\%$, in good agreement with the data, as demonstrated later. The simulations showed that the momentum resolution is slightly momentum-dependent and can be parametrized as

$$\sigma_p/p = 2.4 \times (1.536 - 0.0008184 \times p)(\%) \qquad \text{for} \qquad p > 400\ \text{MeV/c}\,. \tag{4}$$

The geometrical acceptance for η's is strongly momentum-dependent and may be parametrized for the 'central' condition as

$$\epsilon_\eta(p) = (p - 342) \times 8.672 \times 10^{-7} \qquad \text{for} \qquad p \geq 342\ \text{MeV/c}\,. \tag{5}$$

The spectral shapes used later as input for the evaluation do not contain the smearing due to the detector resolution.

The separation of $\eta\omega$ from $\eta\varrho$ using the CPH information is based on the following considerations.

The annihilations $p\bar{p} \to \eta\omega$ with $\omega \to \pi^+\pi^-\pi^0$ and $\eta\varrho$ with $\varrho \to \pi^+\pi^-$ are expected to yield angular distributions for the charged π's with respect to the η direction that are not isotropic but are influenced by spin effects and L-S coupling. For both channels the initial $p\bar{p}$ state is $^3S_1$. Of all possible spin orientations, the only ones favoured are those where the spin of the vector meson points into the $\pm\,\vec{p}_\eta$-direction. Since the decay $\varrho \to \pi^+\pi^-$ involves $\vec{L}_{\pi\pi} = \vec{S}_\varrho$, we expect the emission of these charged pions to be essentially perpendicular to $\vec{p}_\eta$ in the rest frame of the ϱ, and with the ϱ-boost mostly into the $\vec{p}_\varrho = -\vec{p}_\eta$ hemisphere with $p_\perp(\pi^+) = -p_\perp(\pi^-)$. The decay of the ω into three pions is more complicated.

Monte Carlo simulations with a code that includes spin effects [8] have shown that these are indeed important for the $\eta\varrho$ channel but are washed out for $\eta\omega$ and πa_2, so that in practice the resulting angular distributions are indistinguishable from pure phase-space distributions. These studies allowed for defining topological criteria that favour either $\eta\varrho$ or $\eta\omega$. The criteria are as follows:

i) Exactly two counters of CPH had fired. Since the CPH allows only angles in the x-y plane to be measured, the further conditions involve only angles in this plane, i.e. ϕ_1 is the angle between the projected $\vec{p}_\eta$ and $\vec{p}_{\pi_1}$ (see fig. 1).

ii) Condition A (ϱ-suppression): both ϕ_1 and ϕ_2 are either smaller or larger than 180° (this means an unbalanced $p_\perp$ and is hence kinematically impossible for $\eta\varrho$). In the case of $\phi_1 = 180°$ within experimental resolution, ϕ_2 has to be either $\phi_2 \leq 90°$ or $\phi_2 \geq 270°$ (this configuration is unlikely for $\eta\varrho$ because of L-S coupling).

iii) Condition B (ϱ-enhancement): $\phi_1 < 180°$ and $\phi_2 > 180°$. In the case of $\phi_1 = 180°$, within errors, ϕ_2 must be $90° \leq \phi_2 \leq 270°$.

Imposing condition A or B also changes the shape of the $\eta\varrho$ and πa_2 momentum distributions.

An almost complete suppression of $\eta\varrho$ is obtained by requiring no hits in the CPH (CPH = 0). Under this condition, about 9% of the $\eta\omega$ survive owing to $\omega \to \pi^0\gamma$.

Table 1 gives the acceptances for 'central' events and the different CPH conditions. The partial decay rates for $\eta \to \gamma\gamma$ (0.39), $a_2 \to \pi\eta$ (0.145), $\eta \to$ neutrals (0.708), and $\eta' \to$ neutrals (0.166) are obtained from ref. [9]. The $\pi^0 a_2$ channel is assumed to be 26% of all πa_2, as may be deduced from ref. [3].

5. EVALUATION OF THE η MOMENTUM SPECTRA

The η momentum spectra were fitted by a smooth background function and the distributions for the different annihilation channels as obtained from the simulations. The continuous background was fitted by the following empirical function:

$$B(p) = h x^\alpha \exp\{[(x - x_0)\varkappa + 0.5\,\alpha\varkappa/x_0]^2\}\,, \tag{6}$$

with $x = p - p_0$ and $x_0 = p_m - p_0$, and $B(p_m)$ being the maximum of the background function. This choice allows for fitting the branches to the left and right of the maximum independently. The fit parameters were h, α, p_0, p_m, and $\varkappa$. The high-momentum branch was also fitted with polynomials of different orders so as to study systematic effects introduced by the background. MINUIT [10] was used for χ^2 minimization.

Two strategies were followed to overcome the difficulties of separating the $\eta\omega$ and $\eta\varrho$ contributions to the spectra:

i) the CPH $\geq$ 1 spectrum (at least one detected charged particle) and the CPH = 0 spectrum (no charged particle detected) were fitted simultaneously;

ii) the spectra for conditions A and B (ϱ suppression and ϱ enhancement) were fitted simultaneously.

To fit simultaneously the different spectra corresponding to different non-overlapping subsets of the data (different CPH conditions) means that these spectra constitute one single data-set, to be approximated with different backgrounds but with one common parameter for resolution, calibration, and yield for each channel. The relative yields for the different conditions have been fixed according to table 1, and the line shapes are those obtained in section 4.

The line shapes as obtained from the simulations (section 4) were folded with Gaussians representing the detector resolution [Eq. (4)]. The peaks due to annihilations into $\eta\eta'$ (546.10 MeV/c), $\eta\eta$ (761.04 MeV/c), and $\eta\pi^0$ (852.27 MeV/c) were fitted with pure Gaussians with σ's given by the detector resolution [Eq. (4)].

5.1 The CPH $\geq$ 1 and CPH = 0 spectra

The spectra shown in fig. 4 were fitted using the annihilation channels of table 1. Apart from the background parameters, the free parameters were the yields, the detector resolution, and the absolute momentum calibration. Comparing the fitted peak positions for $\eta\varrho$ and $\eta\omega$ with the one expected from the simulations, we found the absolute calibration to be correct to better than 0.2%. The resolution was $\sigma_p/p = 2.43\%$ for the $\eta\omega/\eta\varrho$ peak, which is in reasonable agreement with the Monte Carlo simulation and indicates that the error estimates concerning the detector response [Eqs. (1) and (2)] are correct.

The 'central' and 'total' spectra were analysed independently. When fitting the 'total' spectrum, the momentum-dependent z-cut efficiency [Eq. (3)] was corrected for. The results are shown in table 2. The errors are statistical, as obtained from a MINOS [10] analysis. The spectra and the fits are shown in fig. 4. Various background fits have led to somewhat different values for the ratio of the number of events found for $\eta\varrho$ and $\eta\omega$, and $N_{\eta\varrho}/N_{\eta\omega}$ is within the limits:

$$0.48 \leq N_{\eta\varrho}/N_{\eta\omega} \leq 0.71 \,. \tag{7}$$

These limits determine the systematic errors for the corresponding branching ratios. It should be noted that $N_{\eta\omega}$ and $N_{\pi a_2}$ are correlated with $N_{\eta\varrho}$ so that both decrease with increasing $N_{\eta\varrho}$. The other channels are not sensitive to background differences.

5.2 The spectra for conditions A and B

The spectra for conditions A and B (ϱ suppressed and ϱ enhanced, as described in section 4) were analysed together with the spectrum for CPH $\geq$ 1. The three spectra were analysed simultaneously in order to constrain the $\eta\varrho$ and $\eta\omega$ parameters to values compatible with the CPH $\geq$ 1 spectrum. A systematic χ^2 analysis was performed for a series of different fixed values of $N_{\eta\varrho}/N_{\eta\omega}$. The results are listed in table 3. The spectra for conditions A and B are shown in fig. 5.

5.3 Summary of the analysis

From the previous two sections we deduce the final values as listed in table 4. The errors are statistical (first error) and systematic, introduced through the background fit. Based on the results of subsections 5.1 and 5.2, we have adopted the ratio

$$N_{\eta\varrho}/N_{\eta\omega} = 0.52 \pm 0.05 \,^{+0.19}_{-0.04} \tag{8}$$

5.4 Branching ratios

The branching ratios for the different annihilation channels x are obtained through the following formula:

$$BR_x = N_x/(N_{\bar{p}} \times \epsilon_{\chi 2} \times \epsilon_{acc} \times \epsilon_{conv}) , \tag{9}$$

where

N_x = number of events from channel x,

$N_{\bar{p}}$ = 5.74×10^9, the total number of $\bar{p}$'s,

$\epsilon_{\chi 2}$ = 0.90 ± 0.03, the fraction of events surviving the χ^2 cut of $\chi^2 < 4.45$,

ϵ_{acc} = acceptance for channel x, as from table 1,

ϵ_{conv} = 0.93 ± 0.03, the probability that neither of the two γ's from η decay has converted before reaching the detector.

The different factors entering Eq. (9) had to be determined separately and led to additional common systematic errors. They are discussed in the following subsections.

5.5 The χ^2 cut rejection ($\epsilon_{\chi 2}$)

The χ^2 as obtained from the kinematical fit (section 3) was limited to $\chi^2 < 4.45$. This cut essentially rejects background from uncorrelated γ pairs, i.e. γ's originating from the decay of different particles. Thus the χ^2 cut reduces the total number of events in the spectra by as much as a factor of 2.6, and consequently improves the peak-to-background ratio.

The fact that the measured quantities do not necessarily have normally distributed errors (e.g. γ energies may have long tails towards lower energies) may lead to abnormally large χ^2 values in the kinematical fitting. Hence the losses introduced by the χ^2 cut have to be determined independently.

For this purpose, the uncut η momentum spectrum was fitted with fixed relative yields for the different channels. Only the $\eta\omega$ yield and the resolution were varied. It turns out that of all physical events, $(90 \pm 3)\%$ survive the χ^2 cut.

It is worth noting that for $p_\eta \geq 600$ MeV/c, the 'total' η momentum spectrum contains 31,500 events after χ^2 cutting, whilst the η peak in the invariant mass spectrum (fig. 2), in the same momentum region, contains 24,700 events before cutting. Hence for $p_\eta \geq 600$ MeV/c, the spectrum still contains 29% of uncorrelated background.

5.6 Solid angle (ϵ_{acc})

Whilst the conditions leading to the 'central' spectra confine the detector area in a precise way, the conditions leading to the 'total' spectra have to rely on the accuracy of impact reconstruction for the γ's. In order to check this point, the total number of events in the η spectra, before the χ^2 cut, was determined for the 'total' and the 'central' conditions. The ratio N('total')/N('central') was found to be 1.874, which leads to the conclusion that the effective 'total' condition corresponds to a cut at $|z| \leq 8.794$. The acceptances for the 'total' condition may therefore be obtained by multiplying the acceptances for the 'central' condition (as listed in table 1) by 1.874.

Assuming an error of ± 2 mm for the definition of the 'central' cut ($|z| \leq 6.4$ cm) leads to an overall error of 6% for the acceptances of table 1.

5.7 Gamma conversion (ϵ_{conv})

Given the amount of material that a γ has to traverse (see section 2), there is a finite chance that it converts into an electron-positron pair before it hits the detector. The probability that both γ's survive is estimated to be $(93 \pm 3)\%$.

5.8 Additional systematic errors

Two more sources of systematic errors must be considered:

i) the partial decay rate for $\eta \to \gamma\gamma$ is $(38.9 \pm 0.4)\%$ [9], hence all branching ratios will have an additional error of 1.0%;

ii) the partial decay of $a_2 \to \eta\pi$ amounts to $(14.5 \pm 1.2)\%$ [9]. The branching ratio for $p\bar{p} \to \pi a_2$ will therefore have an additional error of 8.3%.

5.9 Final branching ratios

Based on the results of table 4, the acceptances of table 1, and the correction factors discussed above, we deduce the branching ratios given in table 5. The errors are the statistical and systematic fit errors of table 4, with the systematic errors from the corrections added in quadrature. The correlations of the systematic fit errors are indicated by their relative signs.

6. DISCUSSION AND CONCLUSIONS

6.1 $p\bar{p} \to \eta\rho$ and $p\bar{p} \to \eta\omega$

The branching ratio for $p\bar{p} \to \eta\varrho$ had been measured earlier by Foster et al. [2] to be $(0.64 \pm 0.14)\%$ and by Baltay et al. [1] to be $(0.22 \pm 0.17)\%$. Our value of $(0.53^{\pm 0.20}_{\mp 0.09})\%$ is in agreement with the former, but is about 1.6σ away from the latter. The three measurements together constrain the branching ratio for $\eta\varrho$ to $(0.51 \pm 0.07)\%$. The branching ratio for $p\bar{p} \to \eta\omega$ had not been measured before. Our value of $(1.04^{\pm 0.09}_{\mp 0.10})\%$ constitutes new information in the domain of $p\bar{p}$ annihilations at rest. The accuracy for both branching ratios is limited by the systematic fit error. The two branching ratios are correlated, as indicated by the signs of the errors.

The ratio $BR(\eta\varrho)/BR(\eta\omega) = 0.51^{\pm 0.20}_{\mp 0.06}$ is independent of the systematic errors that are due to the corrections.

Theoretically, these branching ratios are of great value since, because of C-parity conservation, they originate unambiguously from initial $^3S_1$ $p\bar{p}$ states. Three recent theoretical calculations of these branching ratios predict values for $BR(\eta\varrho)/BR(\eta\omega)$ between 0.1 and 1 [11–13].

6.2 $p\bar{p} \to \pi a_2$

Diaz et al. [3] have measured the branching ratios for the channel $p\bar{p} \to \pi^{\pm} a_2^{\mp}$, with $a_2^{\mp}$ decaying into $\varrho^0\pi^{\mp}$ for the initial states $^3S_1$ and $^1S_0$. After correcting for unobserved $\varrho^{\mp}\pi^0$ and for the unseen channel $p\bar{p} \to \pi^0 a_2^0$, and using the partial width of $a_2 \to \varrho\pi$ of $(70.1 \pm 2.2)\%$ [9], we deduce from their paper a branching ratio for $p\bar{p} \to \pi a_2$ of $(7.71 \pm 0.98)\%$.

Espigat et al. [4] have measured the branching ratios for the channel $p\bar{p} \to \pi^{\pm} a_2^{\mp}$, with $a_2^{\mp}$ decaying into $\eta\pi^{\mp}$ and $\eta \to \pi^+\pi^-\pi^0$. After correcting their result for all η and a_2 decays, using the partial widths of $(23.7 \pm 0.5)\%$ for $\eta \to \pi^+\pi^-\pi^0$ and $(14.5 \pm 1.2)\%$ for $a_2 \to \eta\pi$ [9], and after correcting for the unseen channel $p\bar{p} \to \pi^0 a_2^0$, their branching ratio for $p\bar{p} \to \pi a_2$ is $(5.5 \pm 1.6)\%$.

Our result of $(8.49^{\pm 1.05}_{\mp 1.10})\%$ is in good agreement with that of Diaz et al. [3], but is about 1.5σ higher than the value of Espigat et al. [4]. It should, however, be noted that any annihilation of the

type $p\bar{p} \rightarrow \pi + X$, with $X \rightarrow \eta\pi$ and 1000 (MeV/c^2) $\leq m_X \leq m_{a_2}$, may contribute to this branching ratio, since the shapes of the η momentum distributions for such channels are quite similar to the one from πa_2.

6.3 $p\bar{p} \rightarrow \eta\pi^0$, $\eta\eta$, and $\eta\eta'$

The annihilations $p\bar{p} \rightarrow \eta\pi^0$, $\eta\eta$, and $\eta\eta'$ can proceed from initial $p\bar{p}$ P-states only. An observation of these annihilation channels is therefore an indication of the presence of P-wave annihilation in liquid hydrogen.

Our branching ratio of $(1.33 \pm 0.27) \times 10^{-4}$ for $\eta\pi^0$ is a clear indication of such annihilation, and confirms our earlier measurement of $p\bar{p} \rightarrow \pi^0\pi^0$ [14], where a branching ratio of $(2.06 \pm 0.14) \times 10^{-4}$ was found.

In an earlier measurement of the inclusive γ spectra associated with $p\bar{p}$ annihilations in liquid hydrogen [15], a branching ratio of (0.82 ± 0.10)% was found for $p\bar{p} \rightarrow \eta\pi^0$. This value is, however, strongly dependent on the assumption made there, that annihilation channels containing η's (such as $\eta\omega$) were all 16% of the corresponding channels containing π^0's. The present measurement has demonstrated that this assumption was wrong. Hence, a comparison of our result with this earlier one cannot be done without reanalysing the γ spectra of ref. [15].

The branching ratio for the channel $p\bar{p} \rightarrow \eta\eta$ was found to be $(8.1 \pm 3.1) \times 10^{-5}$, and indicates a relative strength of $BR(\eta\eta)/BR(\eta\pi^0) = 0.61 \pm 0.25$.

For the channel $p\bar{p} \rightarrow \eta\eta'$, we obtain an upper limit of $BR(\eta\eta') \leq 1.8 \times 10^{-4}$ at 95% CL.

It should be noted that these branching ratios might be partly due to annihilations in flight, since the $\bar{p}$'s have to traverse about 10 cm of liquid hydrogen before they come to rest (see section 2). However, we may overcome this uncertainty by normalizing to the branching ratio for $\pi^0\pi^0$ [14], which was measured with the same target. We then derive $BR(\eta\pi^0)/BR(\pi^0\pi^0) = 0.65 \pm 0.13$, $BR(\eta\eta)/BR(\pi^0\pi^0) = 0.39 \pm 0.15$, and $BR(\eta\eta')/BR(\pi^0\pi^0) < 0.87$ at 95% CL.

Such ratios have been calculated by Genz [16] and by Dover and Fishbane [17], and may also be obtained from ref. [18].

6.4 Summary

For the first time a high-statistics η momentum spectrum, after $p\bar{p}$ annihilation at rest, could be obtained by direct observation of η's through their decay into two γ's. Branching ratios for $p\bar{p}$ annihilations into $\eta\varrho$, $\eta\omega$, $\eta\pi^0$, $\eta\eta$, and πa_2 were obtained, and an upper limit was derived for the channel $\eta\eta'$. Of these branching ratios, only the ones for $\eta\varrho$ and πa_2 had been measured before.

The availability of precise data on annihilations at rest into $\eta\omega$ and $\eta\varrho$, as well as into two pseudoscalar mesons, as suggested by Dover and Fishbane [17], should contribute to a better understanding of the problems connected with annihilations into two mesons.

Acknowledgements

This work was supported by the Swiss National Science Foundation, by the Swedish Research Council, and by the Greek Administration for Research and Technology. We would like to thank CERN for the hospitality we have received, and the CERN Hydrogen Group of L. Mazzone for constructing and operating the hydrogen target. We are also indebted to K. Agehed and A. Engström (Stockholm), D. Damianoglu and K. Iconomou (Thessaloniki), and F. Abt and H. Krause (Basle) for technical assistance.

REFERENCES

[1] C. Baltay et al., Phys. Rev. **145** (1966) 1103.

[2] M. Foster et al., Nucl. Phys. **B8** (1968) 174.

[3] J. Diaz et al., Nucl. Phys. **B16** (1970) 239.

[4] P. Espigat et al., Nucl. Phys. **B36** (1972) 93.

[5] S. Carius, Ph.D. thesis, Royal Institute of Technology, Stockholm (1986).

[6] L. Adiels et al., Nucl. Instrum. Methods **A244** (1986) 380.

[7] C. Findeisen, Ph.D. thesis, University of Basle (1986).

[8] C. Amsler and J.C. Bizot, Comput. Phys. Commun. **30** (1983) 21.

[9] Particle Data Group, Phys. Lett. **B170** (1986) 1.

[10] F. James and M. Roos, Comput. Phys. Commun. **10** (1975) 343.

[11] J. Vandermeulen, Proc. 4th LEAR Workshop; Physics at LEAR with Low-Energy Antiprotons, Villars-sur-Ollon, 1987, eds. C. Amsler et al. (Nuclear Science Research Conference Series, Harwood Academic Publishers, Chur, 1988), Vol. 14, p. 437.

[12] M. Maruyama and T. Ueda, same Proceedings as ref. [11], p. 425.

[13] A.M. Green and G.Q. Liu, $N\bar{N}$ annihilation into two mesons—effect of final-state interactions, Univ. Helsinki preprint HU-TFT-88-4 (1988).

[14] L. Adiels et al., Z. Phys. **C35** (1987) 15.

[15] G. Backenstoss et al., Nucl. Phys. **B228** (1983) 424.

[16] H. Genz, Phys. Rev. **D28** (1983) 1094.

[17] C. Dover and P. Fishbane, Nucl. Phys. **B244** (1984) 349.

[18] M. Maruyama and T. Ueda, Progr. Theor. Phys. **73** (1985) 1211.

Table 1

Acceptances (in units of 10^{-4}) of the detector system for the different $p\bar{p}$ annihilation channels and for the 'central' condition. Acceptances are quoted for the CPH conditions explained in sections 3 and 4. Decay branching ratios are included.

Channel	CPH $\geq$ 1	CPH = 0	$\eta\varrho$ enhancement	$\eta\varrho$ suppression
$\eta\varrho$	1.077	0	0.2709	0.1749
$\eta\omega$	0.9596	0.09144	0.1359	0.3269
πa_2	0.09050	0.03180	0.02613	0.01418
$\eta\pi^0$	0.0	1.725	-	-
$\eta\eta$	0.8278	2.007	-	-
$\eta\eta'$	0.5754	0.1145	-	-

Table 2

Results of the analysis of the 'central' and 'total' spectra for CPH $\geq$ 1 and CPH = 0; N_x is the number of events for $p\bar{p}$ annihilation channel x. Errors are statistical only. Also quoted are the detector resolution at 650 MeV/c and χ^2/NDF.

	'Central'	'Total'
$N_{\eta\omega}$	5277 $\pm$ 177	9784 $\pm$ 274
$N_{\eta\varrho}/N_{\eta\omega}$	0.483 $\pm$ 0.065	0.523 $\pm$ 0.053
$N_{\pi a_2}/N_{\eta\omega}$	0.949 $\pm$ 0.044	0.956 $\pm$ 0.036
$N_{\eta\pi^0}/N_{\eta\omega}$	0.0203 $\pm$ 0.0042	0.0219 $\pm$ 0.0035
$N_{\eta\eta}/N_{\eta\omega}$	0.0204 $\pm$ 0.0079	0.0215 $\pm$ 0.0085
$N_{\eta\eta'}/N_{\eta\omega}$	0.0 $\pm$ 0.0350	0.0 $\pm$ 0.0065
σ_p/p	(2.43 $\pm$ 0.08)%	(2.49 $\pm$ 0.07)%
χ^2/NDF	1.20	1.39

Table 3

Results of the analysis of the 'central' and 'total'
spectra for conditions A ($\eta\varrho$ suppression) and B ($\eta\varrho$ enhancement).
The ratio of the number of events found for
$p\bar{p} \rightarrow \eta\varrho$ and $\eta\omega$ is quoted.
Errors correspond to $\chi^2_{min} + 1$. Also quoted is χ^2/NDF.

	'Central'	'Total'
$N_{\eta\varrho}/N_{\eta\omega}$	0.528 ± 0.040	0.529 ± 0.040
χ^2/NDF	1.08	1.07

Table 4

Summary of the analysis of the 'central' and 'total' spectra.
Quoted are the number of events N_x for each $p\bar{p}$ annihilation channel x,
the statistical error (first error), and the systematic errors
due to the background fitting.

	'Central'	'Total'
$N_{\eta\omega}$	$5280 \pm 180^{-430}_{+0}$	$9800 \pm 274^{-460}_{+150}$
$N_{\eta\varrho}$	$2746 \pm 137^{+522}_{-110}$	$5096 \pm 255^{+968}_{-204}$
$N_{\pi a_2}$	$5007 \pm 240^{-210}_{+50}$	$9350 \pm 352^{-395}_{+98}$
$N_{\eta\pi^0}$	107 ± 22	214 ± 34
$N_{\eta\eta}$	108 ± 39	210 ± 70
$N_{\eta\eta'}$	0 ± 180	0 ± 64

Table 5

Branching ratios BR (col. 2), in per cent of all annihilations for the different annihilation channels. Quoted are also the statistical error σ_{stat} (col. 3), the systematic error due to the background fitting (col. 4), and the sytematic error σ_{corr} due to corrections (col. 5). The total error (col. 6) is obtained by adding these errors in quadrature. Correlations are indicated by the sign of the errors.

Channel	BR	σ_{stat}	Fit error	σ_{corr}	Total error
$\eta\omega$	1.04	0.03	-0.05 $+0.02$	0.08	-0.10 $+0.09$
$\eta\varrho$	0.53	0.05	$+0.19$ -0.04	0.04	$+0.20$ -0.08
πa_2	8.49	0.36	-0.36 $+0.09$	0.98	-1.10 $+1.05$
$\eta\pi^0$	0.0133	0.0025	-	0.0010	± 0.0027
$\eta\eta$	0.0081	0.0030	-	0.0006	± 0.0031
$\eta\eta'$	0.0	0.011	-	-	-

Figure captions

Fig. 1 Schematic sketch of the experimental set-up. Cross-section perpendicular to the beam at $z = 0$ (a) and along the beam axis at $y = 0$ (b). The x- and y-scales in the LG region are reduced by a factor of 5 with respect to the x- and y-scales in the target region. See section 2 for explanations.

Fig. 2 The invariant mass $m_{\gamma\gamma}$ distribution in the region of the η mass for the 'total' condition and before the χ^2-cut (bin size 4 MeV/c^2). The solid line represents a fit by a Gaussian for the η-mass peak and an empirical background function.

Fig. 3 The η momentum spectrum for the 'total' condition (bin size 4 MeV/c). The peak at 650 MeV/c is due to $p\bar{p} \rightarrow \eta\varrho$ and $\eta\omega$, the shoulder at 800 MeV/c is due to $p\bar{p} \rightarrow \pi a_2$ ($a_2 \rightarrow \eta\pi$). The peak positions due to annihilations into $\eta\eta'$ (546.10 MeV/c), $\eta\eta$ (761.04 MeV/c), and $\eta\pi^0$ (865.27 MeV/c) are also indicated.

Fig. 4 The 'total' η momentum spectra for CPH $\geq$ 1 (a) and CPH = 0 (b), before (top) and after (bottom) background subtraction (bin size 4 MeV/c). Solid lines correspond to the fit. The distributions for $\eta\omega$, $\eta\eta$, and $\eta\pi^0$ (····), for $\eta\varrho$ (----), and for πa_2 (-·-·-) are shown in the bottom figures.

Fig. 5 The 'total' η momentum spectra for $\eta\varrho$ enhancement (a) and $\eta\varrho$ suppression (b) before (top) and after (bottom) background subtraction (bin size 4 MeV/c). Solid lines correspond to the fit. The distributions for $\eta\omega$ (····), for $\eta\varrho$ (----), and for πa_2 (-·-·-) are shown in the bottom figures.

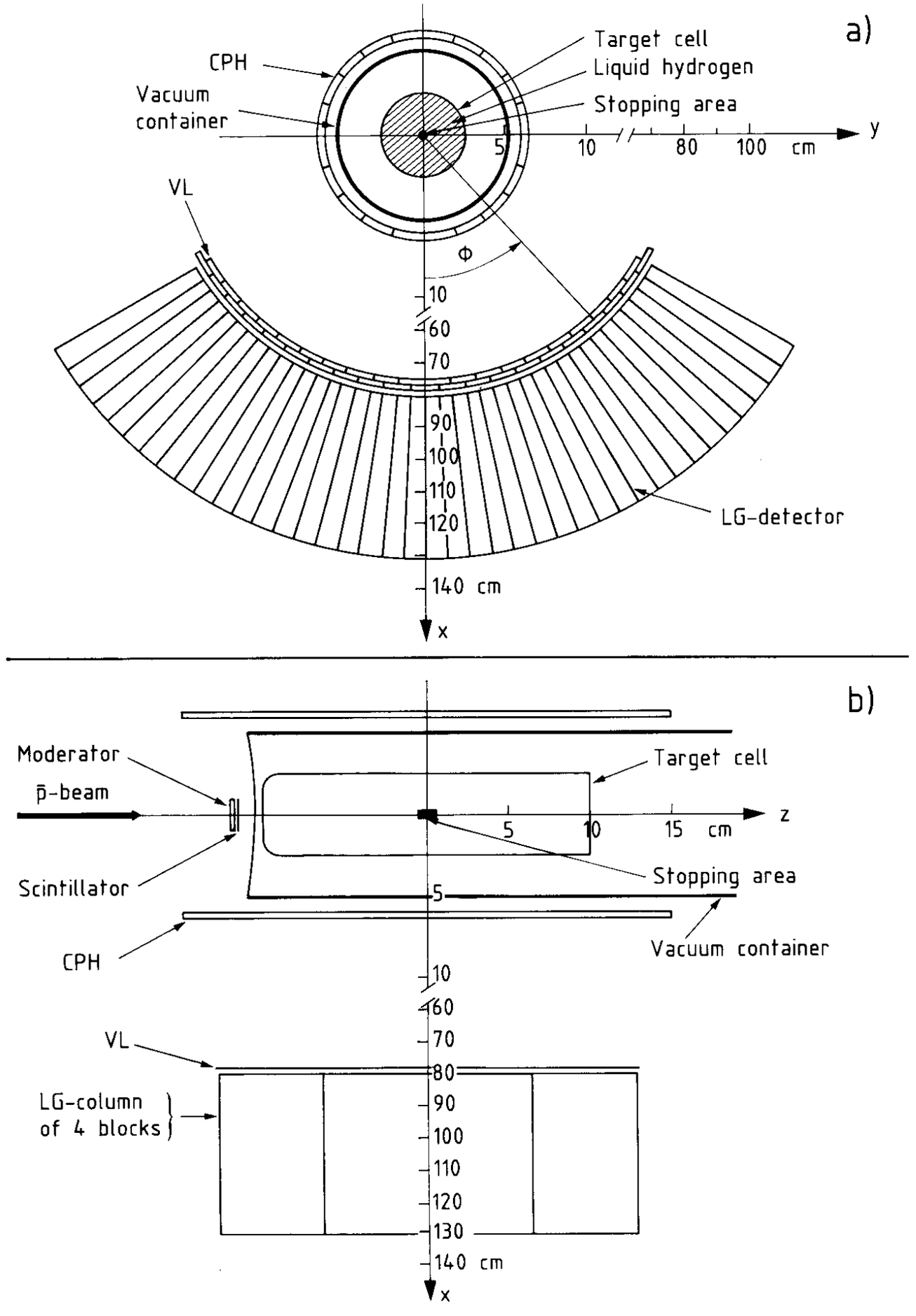
a)
CPH
Vacuum container
Target cell
Liquid hydrogen
Stopping area
y
5
10
80
100
cm
VL
Φ
10
60
70
90
100
110
120
LG-detector
140 cm
x
b)
Moderator
p̄-beam
Target cell
z
5
10
15
cm
Scintillator
Stopping area
5
CPH
Vacuum container
10
60
VL
70
80
LG-column of 4 blocks
90
100
110
120
130
140 cm
x

Fig. 1

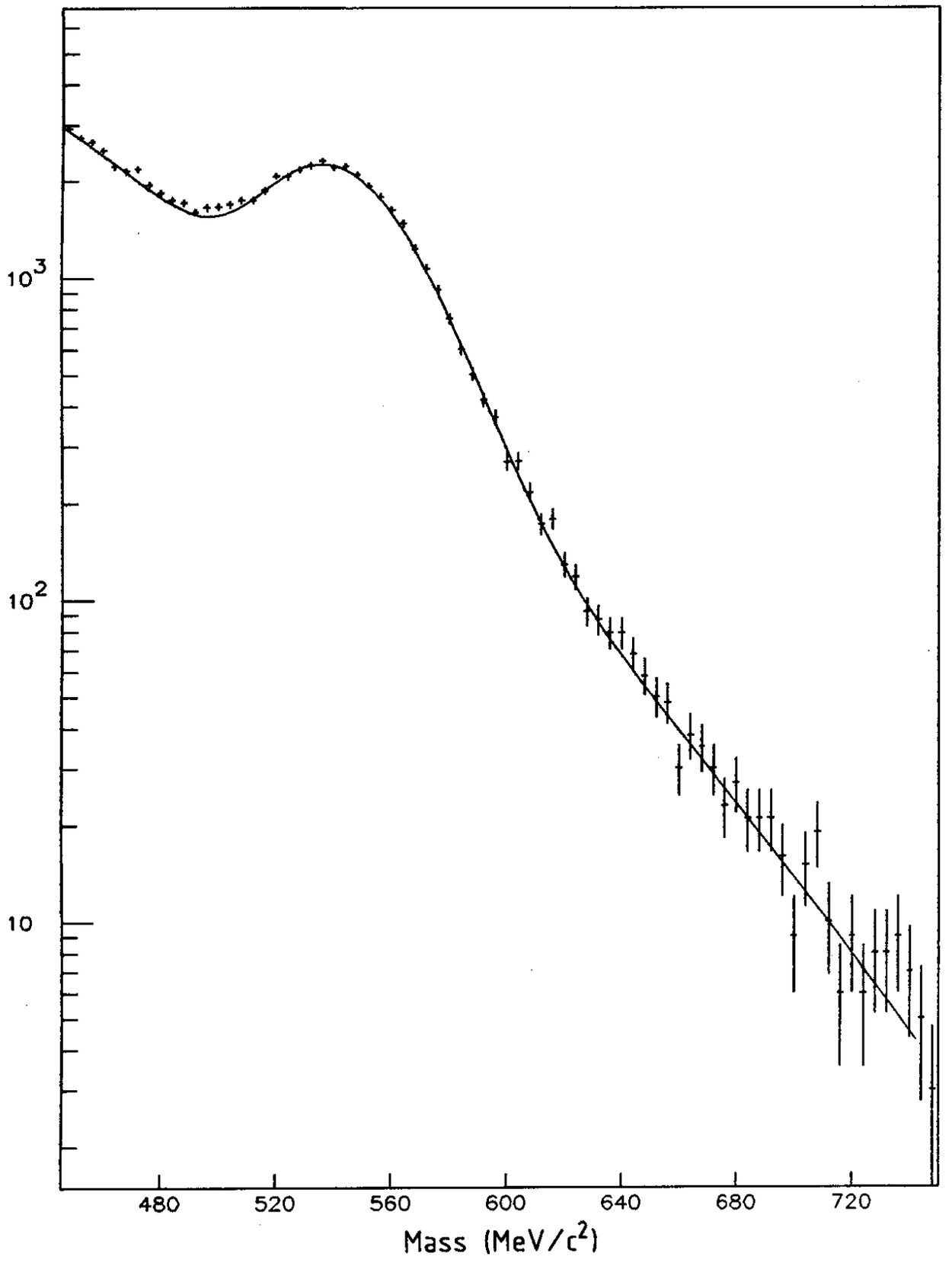

Fig. 2

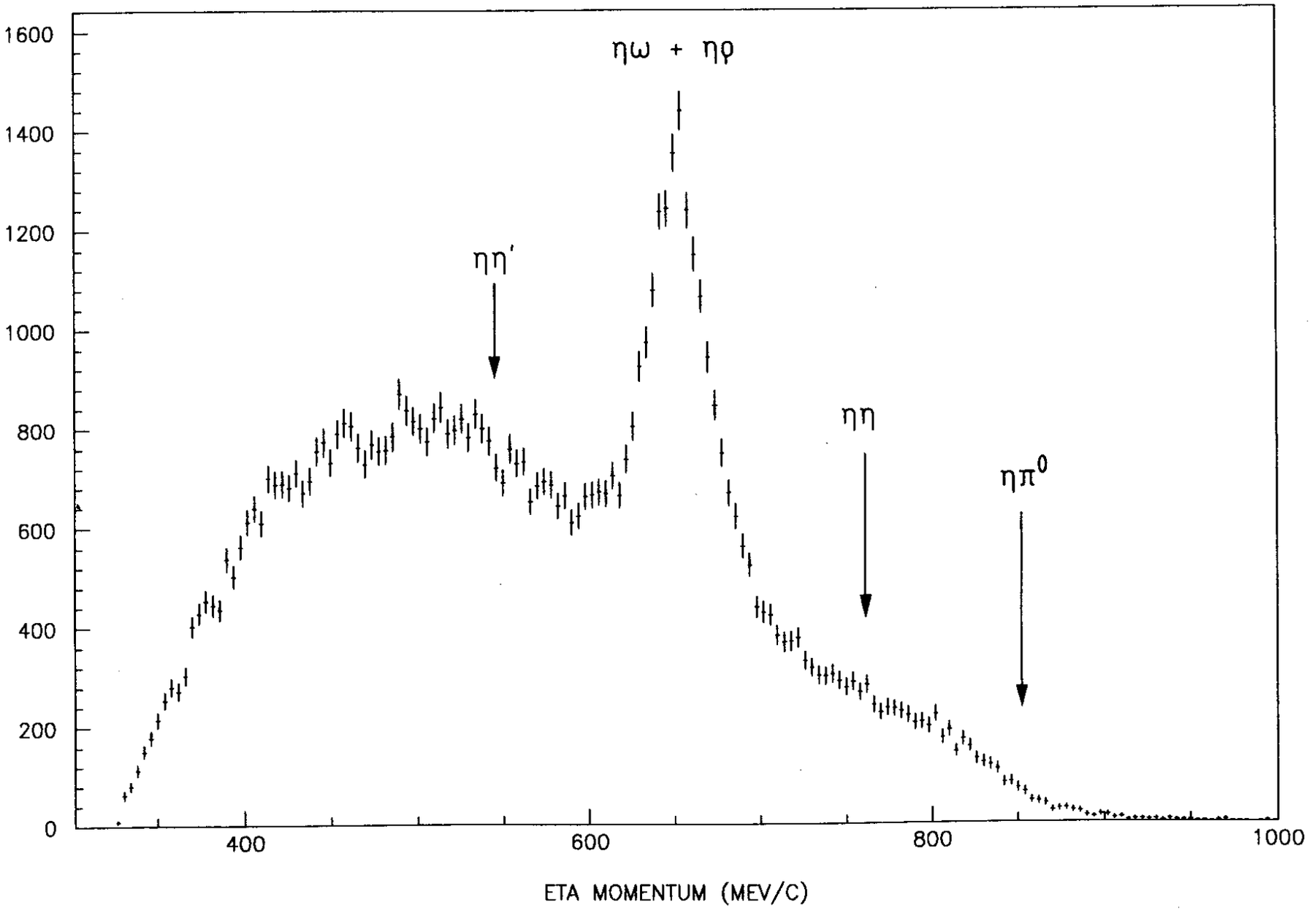
1600
1400
1200
1000
800
600
400
200
0
400
600
800
1000
ηω + ηρ
ηη'
ηη
ηπ0
ETA MOMENTUM (MEV/C)

Fig. 3

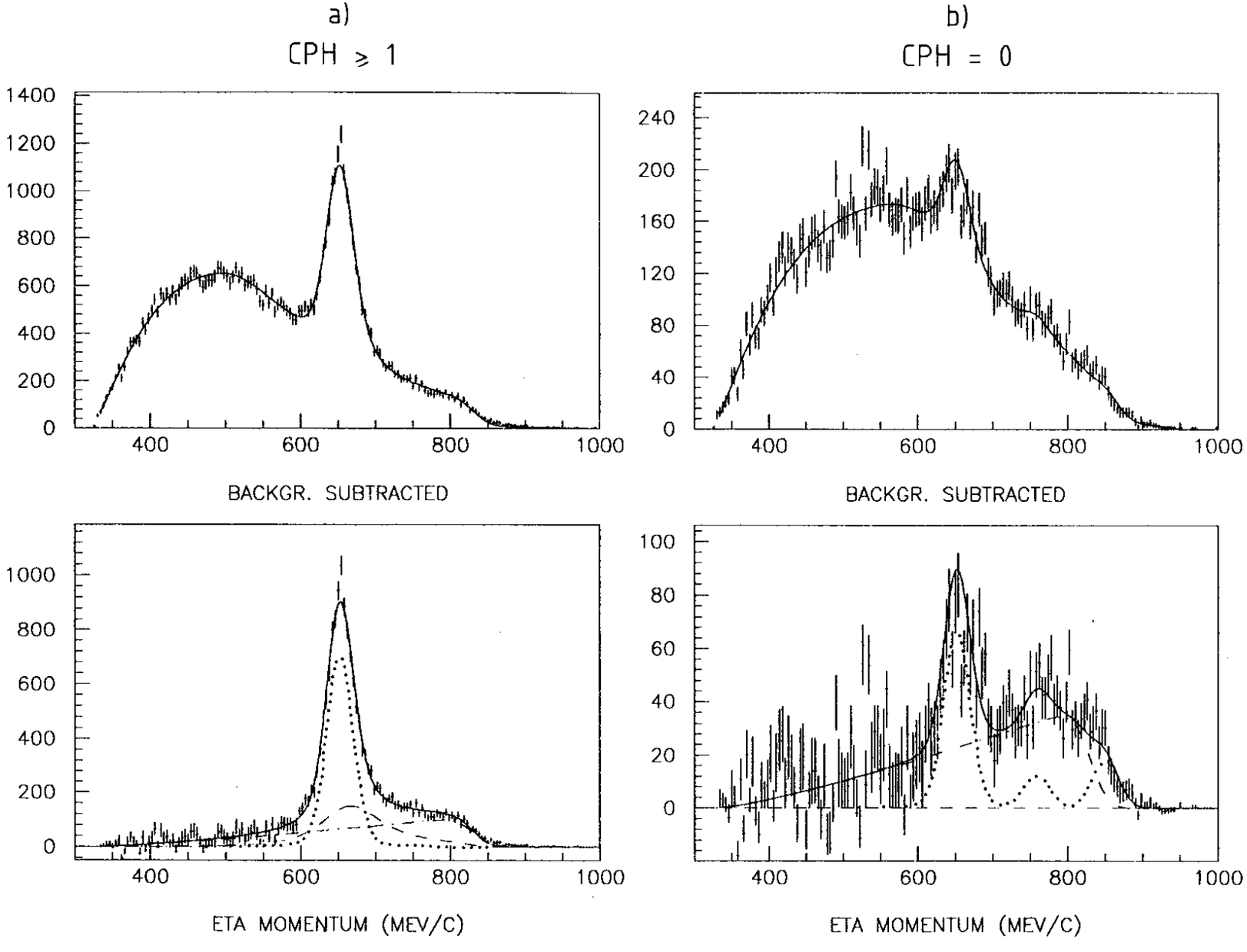
a)
CPH ≥ 1
b)
CPH = 0
BACKGR. SUBTRACTED
BACKGR. SUBTRACTED
ETA MOMENTUM (MEV/C)
ETA MOMENTUM (MEV/C)

Fig. 4

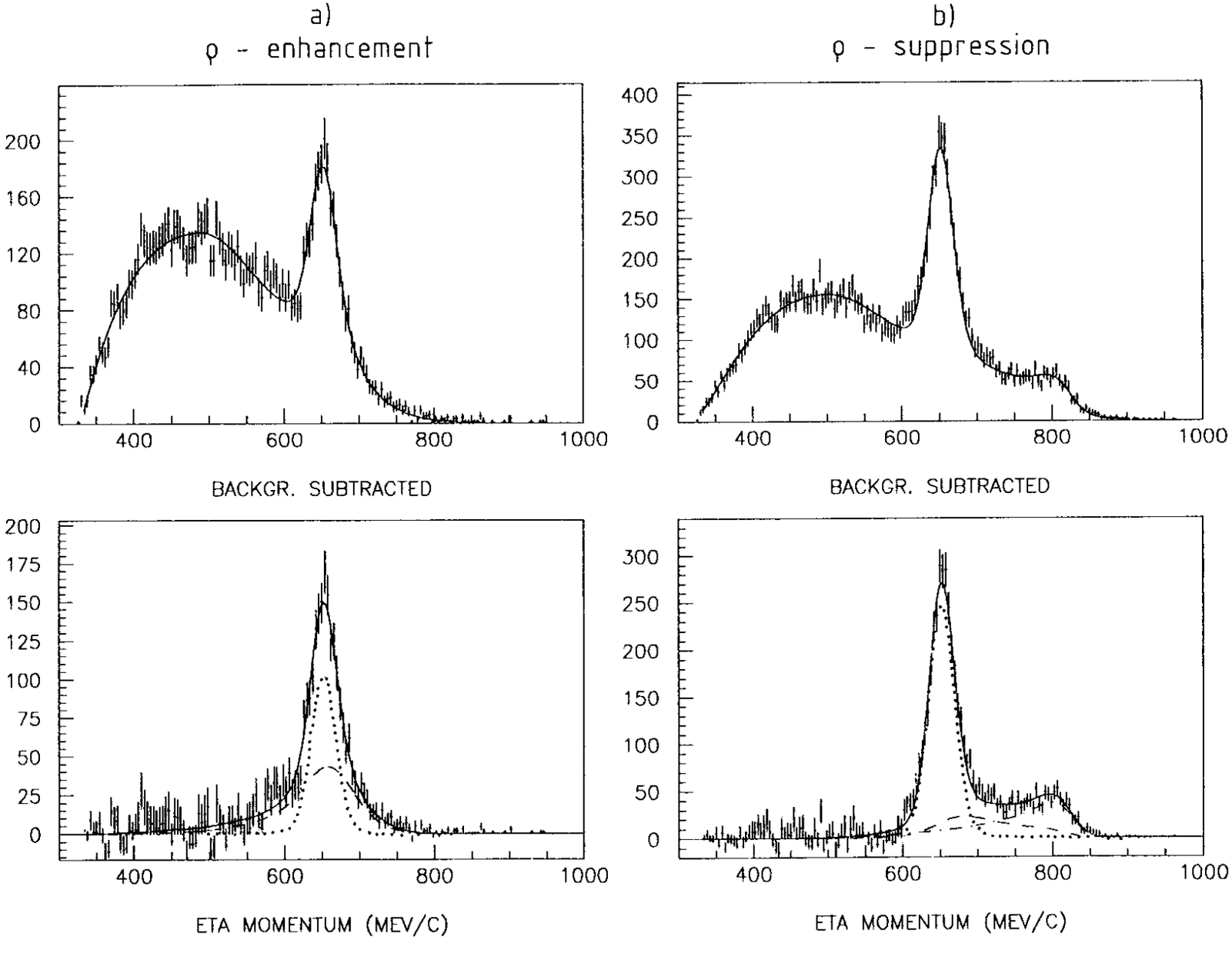
a)
ρ - enhancement
b)
ρ - suppression
BACKGR. SUBTRACTED
BACKGR. SUBTRACTED
ETA MOMENTUM (MEV/C)
ETA MOMENTUM (MEV/C)

Fig. 5